Anharmonic Effects on Vibrational Spectra Intensities: Infrared, Raman, Vibrational Circular Dichroism and Raman Optical Activity

Article *in* The Journal of Physical Chemistry A · November 2015

DOI: 10.1021/acs.jpca.5b10067

CITATIONS
63

READS
673

3 authors:

Julien Bloino
Scuola Normale Superiore di Pisa
102 PUBLICATIONS **17,337** CITATIONS

SEE PROFILE

Malgorzata Biczysko
Shanghai University
131 PUBLICATIONS **4,321** CITATIONS

SEE PROFILE

Vincenzo Barone
Scuola Normale Superiore di Pisa
938 PUBLICATIONS **88,149** CITATIONS

SEE PROFILE

Published in final edited form as:
J Phys Chem A. 2015 December 10; 119(49): 11862–11874. doi:10.1021/acs.jpca.5b10067.

Anharmonic Effects on Vibrational Spectra Intensities: Infrared, Raman, Vibrational Circular Dichroism and Raman Optical Activity

Julien Bloino[*,†], **Malgorzata Biczysko**[*,‡,†], and **Vincenzo Barone**[¶]

[†]Consiglio Nazionale delle Ricerche, Istituto di Chimica dei Composti OrganoMetallici (ICCOM-CNR), UOS di Pisa, Area della Ricerca CNR, Via G. Moruzzi 1, I-56124 Pisa, Italy

[‡]International Center of Quantum and Molecular Structures, College of Sciences, Shanghai University, 99 Shangda Road, Shanghai, 200444 China

[¶]Scuola Normale Superiore, Piazza dei Cavalieri 7, 56126 Pisa, Italy

Abstract

The aim of this paper is twofold. First, we want to report the extension of our virtual multifrequency spectrometer (VMS) to anharmonic intensities for Raman Optical Activity (ROA) with the full inclusion of first- and second-order resonances for both frequencies and intensities in the framework of the generalized second-order vibrational perturbation theory (GVPT2) for all kinds of vibrational spectroscopies. Then, from a more general point of view, we want to present and validate the performance of VMS for the parallel analysis of different vibrational spectra for medium-sized molecules (IR, Raman, VCD, ROA) including both mechanical and electric/magnetic anharmonicity. For the well-known methyloxirane benchmark, careful selection of density functional, basis set, and resonance tresholds permitted to reach qualitative and quantitative vis-à-vis comparison between experimental and computed band positions and shapes. Next, the whole series of halogenated azetidinones is analyzed, showing that it is now possible to interpret different spectra in terms of electronegativity, polarizability, and hindrance variation between closely related substituents, chiral spectroscopies being particular effective in this connection.

Keywords

anharmonicity; VPT2; intensities; IR; Raman; VCD; ROA

1 Introduction

Contemporary chemical research relies more and more on sophisticated experimental techniques, mainly based on rotational, vibrational, electronic, and resonance spectroscopies1–13, allowing the investigation of systems of increasing complexity, e.g. in biology, to identify molecular life mechanisms,14 and in materials science, to search for new

[*] julien.bloino@pi.iccom.cnr.it; biczysko@shu.edu.cn.

Europe PMC Funders Author Manuscripts

materials with tailored/tuneable functionalities.15 Particularly effective routes are established when several spectroscopic techniques are combined together and are further supported by integrated computational approaches. As a matter of fact, spectra do not provide direct access to molecular structure and dynamics, and interpretation of the indirect information that can be inferred from the analysis of the experimental data is seldom straightforward. These complications arise from the inherent complexity caused by thermal or environmental effects and/or from intrinsic properties of the system itself, whose specific roles are not easy to separate and evaluate. In this context, computational spectroscopy is becoming a powerful and reliable tool to help unravel the various contributions to the spectroscopic signal, allowing a deeper understanding of the underlying phenomena.[2,7,9,16–25]

Till now vibrational computations for all but the smallest molecules[26–31] are still mainly performed within the double harmonic approximation, possibly employing simple scaling factors[32–37] or more sophisticated scaling methods[32,38,39] to improve the agreement with anharmonic fundamental transitions. However, such approaches can correct at best the band positions, but have little effect on the general pattern of the harmonic spectrum. Only the explicit inclusion of anharmonic contributions can provide more realistic spectral patterns and either variational[40–43] or perturbative[44–53] routes can be followed to this end. However, all computations which do not take into account anharmonic effects on the transition moments do not provide any information about the intensities of overtones and combination bands, or the intensity re-distribution of fundamental transitions, which might be necessary to correctly analyze experimental outcomes. The most obvious cases are spectral ranges where only non-fundamental transitions are present, either in mid-IR range (i.e. the 1700-2800 cm^{-1} range for napthalene[54] or methyloxirane[55]) or in the near-infrared (NIR) region.[54,56–58] However, fully anharmonic computations are also needed to distinguish low-intensity features related to non-fundamental transitions of the most populated species present in experimental mixtures from fundamental transitions of the less abundant ones.[59–62] The situation becomes even more involved for chiroptical spectra, where anharmonic effects might modulate the observed overall band-shape. However, in most of the contemporary computational studies the anharmonic effects are still at best applied to the energies.

Direct vis-à-vis comparison between simulated and computed spectra can be greatly facilitated by the development of computational models for anhamonic vibrational computations, along with their implementation into computational packages.[40,41,43–49] In particular, in our group we are actively developing a virtual multi-frequency spectrometer (VMS),[23,63,64] providing user-friendly access to the latest developments of computational spectroscopy.[54,65–71] The section of VMS in charge of vibrational spectroscopy[54,65–67] has been already successfully applied to the study of Infrared (IR), Raman and vibrational circular dichroism (VCD) spectra of molecular systems of different sizes and complexities, in gas phase, and in other environments (see for instance Refs.[25,55,58,62,72–77]). The present work is devoted to the extension of the VMS capabilities to the simulation of fully anharmonic Raman Optical Activity (ROA) spectra with a proper account of first- (1-2) and second- (1-1, 2-2, 1-3) order resonances in a perturbative/variational evaluation of both frequencies and intensities.

In this context, the vibrational spectra of (*R*)-methyloxirane (MeOx, see Figure 1) recorded in gas phase78,79 or low-temperature matrices76,80 permit a direct comparison with theoretical results, without any strong environmental perturbation within the fingerprint region. For infrared spectra, it has been shown that a very good agreement with experiment, for both band positions and intensities, can be obtained by coupling harmonic calculations at the Coupled Cluster (CC) level with anharmonic effects computed by density functional theory (DFT).55 However, obtaining accurate VCD spectra, which require both electric and magnetic dipole moments, has proven more challenging. Indeed, extensions of CC to compute the atomic axial tensor have been proposed81,82 but not implemented to the best of our knowledge. As a result, simulations of VCD spectra are commonly performed at the DFT level,76 with some uncertainty on the reliability of the methodology. In the present work we will apply the highly accurate CC/DFT force field along with the DFT-based property potential to simulate ROA spectra of methyloxirane in gas phase.

These new developments allow an extensive characterisation through multiple spectroscopies (e.g. IR, Raman, VCD and ROA) in a way similar to what is now commonly done experimentally. In this framework, an effective computational strategy will be applied to analyze substituent effects in β-lactams, a class of molecules showing remarkable biological activity.83 The (R)-4-X-2-azetidinone derivatives (X=F, Cl, Br, see Figure 1), the simplest chiral compounds from this family, have been already selected as model systems in systematic computational investigations of structural, IR, Raman, VCD, and resonance ROA features84,85 within the rigid-rotor / harmonic-oscillator (RRHO) model, pointing out a significant tuning of spectral properties by the halogen substituent. Here, we will extend this analysis to a more refined model including both mechanical and electric/magnetic anharmonicities for IR, Raman and VCD together with far-from-resonance Raman Optical Activity.

The paper is organized as follows: we start from a brief description of the theoretical framework underlying the anharmonic vibrational computations, with particular focus on ROA intensities (section 2), followed by the computational details (section 3). Then, the fully anharmonic IR, Raman, VCD and ROA spectra of methyloxirane are presented and compared with experimental results in section 4.1, while anharmonic effects on the spectral line-shape, considering both band positions and intensities, are discussed taking (R)-4-fluoro-2-azetidinone as a test case. Finally fully anharmonic spectra computed for (R)-4-X-2-azetidinones (X=F, Cl, Br) are discussed in section 4.3, highlighting advantages of our integrated vibrational model for the analysis of vibrational features. General conclusions and perspectives are outlined in the last section.

2 Theory

2.1 ROA intensities

In order to simulate a broad range of spectroscopies at the VPT2 level, the general framework presented in Refs54,66 has been used here. The basic principle is to construct a generic property, ***P***, defined in such a way as to represent either properties functions of the normal coordinates (***q***) or their conjugate momenta (***p***),

Europe PMC Funders Author Manuscripts

$$\boldsymbol{P}=\boldsymbol{P}^{(0)}+\boldsymbol{P}^{(1)}+\boldsymbol{P}^{(2)} \quad (1)$$

$$\boldsymbol{P}^{(0)}=\boldsymbol{P}^{\mathrm{eq}}+s_0\sum_{i=1}^{N}\boldsymbol{P}_i(a_i^{\dagger}+\mathrm{S}a_i) \quad (2)$$

$$\boldsymbol{P}^{(1)}=s_1\sum_{i=1}^{N}\sum_{j=1}^{N}\boldsymbol{P}_{ji}q_j(a_i^{\dagger}+\mathrm{S}a_i) \quad (3)$$

$$\boldsymbol{P}^{(2)}=s_2\sum_{i=1}^{N}\sum_{j=1}^{N}\sum_{k=1}^{N}\boldsymbol{P}_{jki}q_jq_k(a_i^{\dagger}+\mathrm{S}a_i) \quad (4)$$

where $a_i^{\dagger}$ and a_i are respectively the creation and annihilation operators. s_0, s_1 and s_2 are constant factors and S corresponds to a sign, represented as either +1 or -1.

This function is then used to obtain analytic formulas for the transition moments up to 3 quanta54 and can be simply related to the property of interest by identifying the variables in eqs. 2–4 with the actual quantities. The case of IR, VCD and Raman has already been discussed before,25,54,66 so we will focus here on the extension of our framework to ROA.

Raman optical activity is measured as the difference between Raman scatterings associated to right (R) and left (L) circularly polarized lights. However, at variance with VCD for instance, the measurement setup is not unique, as either the incident (incident circular polarization, ICP) or the scattered (SCP) radiation beams can be modulated to get the right and left circular polarization states. Alternatively, both beams can be simultaneously modulated (dual circular polarization, DCP), either in-phase ($\mathrm{DCP_I}$) or out-of-phase ($\mathrm{DCP_{II}}$). Furthermore, several scattering geometries and polarizations can be chosen for the measurements. Indeed, the scattered beam can be measured at different angles with respect to the incident beam, along the same direction (0°, forward scattering), in the opposite direction (180°, backward scattering or backscattering), or at right angle (90°, right-angle scattering) for instance, and different orientations of the linear polarization analyzer can be chosen. The most common scattering setups are summarized in table 1, as well as the symbol used to represent them.

An important simplification to the theoretical problem, used here as well, is to consider that the measurement is done far from resonance. Hence, the present formulas and the relative discussions should only be applied to such cases. Near-resonance conditions require a different development (see for instance Refs.85,86 for discussions on this matter).

ROA was first predicted theoretically by Barron and Buckingham.87 Successive works contributed to a comprehensive definition of the physical bases underlying the various kinds of measurements of ROA intensities (see Refs.6,88–92 for reviews on the subject). Of particular interest in the present work, ROA and Raman intensities have been derived for a large number of measurement setups by Hecht and Nafie.93 Those formulas can be significantly simplified in the far-from-resonance regime. In this context, ICP and SCP provide equivalent information, which differ from DCP. An interesting feature of the latter, in the in-phase, backscattering configuration, is that it can be used to eliminate all isotropic configurations.90,93

Based on these simplifications, it is more convenient to use the notation of Barron and coworkers90 than the general one employed in Ref.93 The formulas for the most common types of scatterings and measurements contributions are reported in table 2.

Hence, the Raman and ROA intensities can be directly related to the isotropic invariants, α and G', and the symmetric anisotropic invariants, $\beta(\alpha)^2$, $\beta(G')^2$, $\beta(A)^2$, given by,

$$\alpha=\frac{1}{3}\langle\alpha_{\tau\tau}\rangle_{I,F}=\frac{1}{3}\sum_{\tau=x,y,z}\langle\alpha_{\tau\tau}\rangle_{I,F} \quad (5)$$

$$G'=\frac{1}{3}\left\langle G'_{\tau\tau}\right\rangle_{I,F}=\frac{1}{3}\sum_{\tau=x,y,z}\left\langle G'_{\tau\tau}\right\rangle_{I,F} \quad (6)$$

$$\beta(\alpha)^2=\frac{1}{2}\sum_{\tau,\eta=x,y,z}\left(3\langle\alpha_{\tau\eta}\rangle_{I,F}\langle\alpha_{\tau\eta}\rangle_{I,F}-\langle\alpha_{\tau\tau}\rangle_{I,F}\langle\alpha_{\eta\eta}\rangle_{I,F}\right) \quad (7)$$

$$\beta\left(G'\right)^2=\frac{1}{2}\sum_{\tau,\eta=x,y,z}\left(3\langle\alpha_{\tau\eta}\rangle_{I,F}\left\langle G'_{\tau\eta}\right\rangle_{I,F}-\langle\alpha_{\tau\tau}\rangle_{I,F}\left\langle G'_{\eta\eta}\right\rangle_{I,F}\right) \quad (8)$$

$$\beta(A)^2=\frac{1}{2}\sum_{\tau,\eta,\varsigma,\rho=x,y,z}\omega_0\langle\alpha_{\tau\eta}\rangle_{I,F}\epsilon_{\tau\varsigma\rho}\langle A_{\varsigma\rho\eta}\rangle_{I,F} \quad (9)$$

ω_0 is the incident wavenumber, and $\epsilon_{\tau\eta\varsigma}$ is the alternating (or Levi-Cività) tensor, defined by the following relations:

$$\epsilon_{xyz}=\epsilon_{zxy}=\epsilon_{yzx}=1$$
$$\epsilon_{zyx}=\epsilon_{xzy}=\epsilon_{yxz}=-1$$
$$\text{all other components are null.}$$

Hence, the definition of the ROA invariants requires the calculation of the transition moments of 3 quantities,

- $\boldsymbol{\alpha}$: the electric dipole-electric dipole tensor, i.e. the polarizability tensor
- $\boldsymbol{G'}$: the electric dipole-magnetic dipole optical activity tensor
- $\boldsymbol{A}$: the electric dipole-electric quadrupole tensor

As stated before, thanks to the general formulation used to compute the transition moment $\langle \boldsymbol{P} \rangle_{I,F}$ at the VPT2 level, extension to the previous quantities requires simply to build a list of equivalence relations, as given in table 3,

2.2 Resonances

As extensively discussed in the literature,44,47,48,52,65,66 VPT2 energies and transition moments can be plagued by resonances. The main issue for energies is the potential presence of Fermi resonances (FR), also labeled 1-2 resonances since they involve the creation of 1 quantum and the annihilation of 2 quanta, or conversely. Several strategies have been proposed to deal with this problem, also by our group.48,50,65,95,96 The most commonly used approach, referred to here as deperturbed VPT2 (DVPT2), is to first identify and remove the resonance. In this work, this is done through a double test, first on the magnitude of the wavenumber difference $\left(|\Delta\omega| \leq \Delta_{\omega}^{1-2}\right.$, with "$\Delta\omega = \omega_i - 2\omega_j$" for type I resonances and "$\Delta\omega = \omega_i - (\omega_j + \omega_k)$" for type II), then on the difference between the VPT2 term and the result from a model variational calculation, the so-called Martin test.95 Successively, the resonant terms, removed from the VPT2 treatment are reintroduced through variational computations, leading to the generalized VPT2 (GVPT2).

This approach is often insufficient to properly account for all anharmonic effects. Indeed, other types of resonances might occur, collectively called Darling-Dennison resonances (DDR) in reference to the first extensive study on one of those types.97 At variance with FR, their presence does not directly impact the calculation of the vibrational energies, and the resonant terms need to be included as a variational treatment. As a result, their study has been scarcer. They are generally classified and labeled based on the number of quanta created and annihilated between the states involved in the resonance, "1-1", "1-3" and "2-2". The actual definition of the different DDR has been studied by different authors.52,97–102 The revised equations proposed by Rosnik and Polik52 have been used here to identify the resonant terms. An important difficulty to their correct evaluations is the potential presence of Fermi resonances in those equations. In order to treat consistently those occurrences already noted by others,99,102 an adapted version of our hybrid degeneracy-corrected PT2/VPT2 method (HDCPT2), introduced for the calculation of vibrational energies65 was chosen. The idea behind the degeneracy-corrected approach (DCPT2) is to replace all potentially resonant terms by a non-divergent form, following the transformation,

$$\frac{Sk^2}{2\Delta\omega} \rightarrow S(\sqrt{\Delta\omega^2+k^2} - \Delta\omega) \quad (10)$$

where S is the sign of "$k^2\Delta\omega$", k^2 is a term containing a product of cubic force constants, and $\Delta\omega$ is a frequency difference, which can be very small in case of Fermi resonances. Since the relation in eq. 10 can be also derived from the Taylor expansion of $\sqrt{\Delta\omega^2+k^2}$, its application can be extended to the calculation of Darling-Dennison resonances as well. HDCPT2 compensates the error of DCPT2 far from resonance by introducing a transition function between DCPT2 and VPT2 (see Ref.65 for details). It should be noted that Krasnoshchekov and collaborators have proposed an alternative approach directly embedded in their on-the-fly canonical Van Vleck perturbation calculations.102,103

Similarly to FR, the test to identify DDR terms is done sequentially in two steps, first on the frequency difference, then on the magnitude of the off-diagonal term,

1. $|\Delta\omega| \leq \Delta_{\omega}^{\mathrm{DD}}$
2. $|\ \langle v' \mid \hat{\mathcal{H}} \mid v'' \rangle\ | \geq K^{\mathrm{DD}}$

where the superscript "DD, v', v''" refers to the type of Darling-Dennison resonance, with $\hat{\mathcal{H}}$ the appropriate vibrational Hamiltonian.

Like vibrational energies, the formulas used for the transition moments are directly impacted by FR, but also by DDR, namely 1-1 for fundamental bands and 1-3 for 3-quanta transitions. While the procedure described above is able to treat satisfactorily most resonant terms for the transition intensities as well, provided the thresholds have been properly set, it may be insufficient in some cases. Indeed, an off-diagonal term (variational correction) of low magnitude would have a small-to-negligible impact on the energies, and so may not pass the second step of the previous test. However, in some critical cases, where the frequency difference is very small, sometimes below 1 cm^{-1}, such a term can have a significant impact on transition intensities due to the differences in the forms of the terms involved in energies and intensities equations. In order to catch such situations as well, a complementary test is added to the second step, where the off-diagonal term is scaled down by the inverse squared wavenumber difference,

$$\left|\frac{\langle v' |\hat{\mathscr{H}}| v'' \rangle}{\Delta\omega^2}\right| \geq K_I^{\mathrm{A-B}}$$

where "A-B" in superscript represents the type of resonance, which can be either "1-1" or "1-3", which are the two kinds of DDR directly involved in intensity calculations. Tests on the molecule studied in this work have shown that $K_I^{\mathrm{A-B}}$ can be set to be one order of magnitude lower than $K^{\mathrm{A-B}}\left(K_I^{\mathrm{A-B}}=K^{\mathrm{A-B}}/10\right)$. A more systematic and technical discussion on resonances will be deferred to a future work.

Once the resonant terms are identified, variational correction to the VPT2 energies and intensities within the GVPT2 approach is done as follows. A symmetric (or hermitian if degenerate modes are present) matrix is built, containing all states of interest. The deperturbed energies are computed and placed on the diagonal of this matrix. Next, off-diagonal terms corresponding to the Fermi or Darling-Dennison resonant terms are added. It

should be noted that in this configuration, only couplings between the states of interest in the simulation are included and interactions with higher-quanta states are ignored. The matrix is then diagonalized and the eigenvalues correspond to the final, GVPT2 vibrational energies. The eigenvectors ($\boldsymbol{L}_E$) are used to project the deperturbed transition moments on the variationally corrected states, following the procedure described in Ref.47

$$\langle \boldsymbol{P} \rangle_{I,F}^{\mathrm{var}} = \boldsymbol{L}_E{}^T \langle \boldsymbol{P} \rangle_{I,F}^{\mathrm{VPT2}} \quad (11)$$

3 Computational details

Density Functional Theory (DFT) was employed to compute equilibrium geometries, quadratic, cubic and semi-diagonal quartic force fields together with first, second, and semi-diagonal third derivatives of the electric field, magnetic field and mixed properties, needed for the computation of fully anharmonic IR, Raman, VCD and ROA spectra at the VPT2 level. For Raman and ROA spectra the chosen configuration will be backscattering with modulation of the scattered beam ($\Delta_{\mathrm{SCP}}(180°)$). We also note that all studied systems satisfy the far-from-resonance regime, with the lowest excited electronic states lying above 5 eV (250 nm),69,85 to be compared with incident frequency of 532 nm. In view of its efficiency and reliability for prediction of structural parameters,60,104,105 vibrational wavenumbers55,62,105–107 along with IR and Raman intensities,25,60,72 the standard functional B3LYP108 has been employed in conjunction with the SNSD polarized basis set of double-ζ quality supplemented by diffuse functions,25,72,109 and including Stuttgart-Dresden core pseudopotentials110,111 for bromine. All equilibrium structures have been obtained using tight convergence criteria (maximum forces and displacements smaller than 1.5×10^{-5} Hartree/Bohr and 6×10^{-5} Å, respectively) for geometry optimisation. The energy and property derivatives at energy minima including mechanical and electric/magnetic anharmonicities, were determined by numerical differentiations of analytic force constants and first derivatives of the electric and magnetic dipoles, and the frequency-dependent electric dipole-electric dipole, electric dipole-magnetic dipole optical activity and electric dipole-electric quadrupole tensors, at displaced geometries along the normal coordinates (with a 0.01 Å step). To get accurate results, all computations were carried out with an ultrafine integration grid (99 radial shells and 590 angular points per shell) to integrate the exchange-correlation kernel. Basis set effects were investigated for methyloxirane by employing the aug-cc-pVTZ basis set.112 For all computations the following thresholds have been employed for the Fermi and Darling-Dennison type resonances: $\Delta_{\omega}^{1-2} = 200\mathrm{cm}^{-1}$ and $K^{1\text{-}2}$=3 cm^{-1}; $\Delta_{\omega}^{\mathrm{DD}} = 100\mathrm{cm}^{-1}$ and K^{DD}=10 cm^{-1}, respectively.

The force field of methyloxirane has been improved by employing a hybrid scheme, which assumes that the differences between vibrational frequencies computed at two different levels of theory are mainly due to the harmonic terms (see, for instance, Refs. 25,57,65,106,113,114). In the present case the hybrid force field was obtained in a normal-coordinate representation by adding the cubic and semi-diagonal quartic B3LYP/SNSD force constants to the best-estimated theoretical harmonic frequencies55 obtained by the so

called “cheap”55,60 composite scheme based on the coupled-cluster computations (at the CC singles and doubles augmented by a perturbative treatment of triple excitations, CCSD(T)115) in conjunction with the cc-pVTZ112,116,117 basis set.

All calculations have been carried out employing a development version of the GAUSSIAN suite of programs.118 Assignments of vibrational modes were performed by means of visual inspection of the atomic displacements along normal modes and by comparison with the assignments reported in the literature. A graphical user interface (VMS-Draw)119 has been used to visualize normal modes and analyze the outcome of vibrational computations.

4 Results and Discussion

4.1 Theoretical and experimental IR, Raman, VCD and ROA spectra of (R)-methyloxirane

Benchmark studies for a large number of molecules have shown that the B3LYP/SNSD model provides reliable harmonic values and accurate anharmonic contributions for vibrational energies, IR intensities and Raman Activities.25,65,72,106 For the specific case of methyloxirane55 the B3LYP/SNSD harmonic wavenumbers and IR intensities show mean absolute errors (MAE) with respect to the best theoretical estimates (CCSD(T)/cc-pVTZ computations corrected for basis-set extrapolation and core correlation by means of the ”cheap” scheme55) of about 12 cm^{-1} and 2 km mol^{-1}, respectively. The B3LYP/SNSD anharmonic wavenumbers show MAE and maximum deviations (|MAX|) with respect to experiment of 12 cm^{-1} and 32 cm^{-1}, while improved agreement, with MAE and |MAX| of 5 cm^{-1} and 18 cm^{-1}, respectively, has been obtained by coupling the harmonic coupled cluster (“cheapCC”) values with anharmonic contributions computed at the B3LYP/SNSD level.55 The CC/B3LYP force-field, validated by comparison with the well resolved IR spectra,76 ensures a high accuracy for the band positions of Raman, VCD and ROA spectra. The situation is more complex for intensities, which in addition to the electric dipoles require, depending on the specific spectroscopy, also magnetic moments, frequency-dependent polarizabilities, frequency-dependent optical rotations, and frequency-dependent dipole-quadrupole tensors. Unfortunately, in most cases, reference high-level post-Hartree-Fock computations (i.e. at the CCSD(T) level with extended basis sets) are not yet feasible for these properties. In fact only recently the first calculations of harmonic ROA spectra using coupled-cluster theory have been reported by Crawford and Ruud,120 resorting to the CC singles and doubles excitations (CCSD) and double-ζ basis set. Furthermore, some spectra (like VCD) require not only the values, but also the relative orientations of the derivatives of electric and magnetic moments. Considering that the very few studies available on Raman and ROA intensities have shown that the effects due to the electron correlation are less pronounced than those originating from the truncation of the basis set,121 DFT approaches are more effective than their MP2 counterparts,122 and the B3LYP functional performs well with comparison to CCSD,120,123 in the present work we will resort to B3LYP computations for all properties, performing a test on basis set convergence of line-shapes for IR, Raman, VCD, and ROA spectra.

The most accurate CC/B3LYP force fields, are obtained combining the best theoretical estimates of harmonic frequencies from Ref.55 with B3LYP/SNSD and B3LYP/aug-cc-pVTZ anharmonic corrections, which are further combined with property surfaces computed

Europe PMC Funders Author Manuscripts

at the B3LYP level with the same basis sets. The fully anharmonic IR, Raman, VCD and ROA spectra presented in Figure 2 show a very good agreement with respect to experiment[76,79] for both basis sets, confirming the effectiveness of the relatively small SNSD basis set. Moreover, the results reported in the present work, which involve variational contributions to intensities together with modified resonance criteria, fully confirm the results and analysis already presented in previous works for IR[55] and VCD[76] spectra. However, some improvements are also observed, as an example, the variational correction due to the 1-1 resonance between ring C–C stretching (υ_{20} at 834 cm^{-1}) and CH_2/CH_3 rocking (υ_{19} at 894 cm^{-1}) leads to the redistribution of the VCD signal, in agreement with experiment (see Figure 3). The increased number of variational contributions, which can be now taken into account (6 Fermi and 80 Darling-Denison (6 (2-2), 12 (1-1) and 62 (1-3)) resonances) leads also to a remarkably robust procedure with a strongly reduced dependence on specific threshold values.

The ROA spectra presented in Figure 4, show that anharmonic computations convoluted with the larger band-width yield spectra pattern in good agreement with the experimental spectrum recorded in the gas phase,[79] which is characterized by rather broad bands and is complicated by low signal-to-noise ratio and a not-fully resolved rotational structure.[79] On the contrary, harmonic computations show larger discrepancies, with bands noticeably shifted and several transitions missing, while clearly visible in the anharmonic ROA spectrum at higher resolution. Considering the experimental challenge of ROA measurements in the gas phase due to the low sensitivity of the scattering technique,[79] the availability of fully anharmonic theoretical spectra represents a viable alternative for obtaining reference ROA spectra of isolated systems, which, in turn, allow to put in evidence the environmental effects present in condensed phases.

4.2 Anharmonic effects on IR, Raman, VCD and ROA spectra: the case of (R)-4-fluoro-2-azetidinone

As mentioned in the introduction, anharmonic effects on the transition intensities can have an important impact on the overall spectral band-shape, in particular for the chiroptical spectroscopies. In this and the following section these aspects will be analyzed using azetidinone derivatives as test cases. This class of molecules is attracting increasing interest in view of the remarkable pharmacological properties of some of its members and their semi-rigid structure ensures the reliability of perturbative treatments based on polynomial representations of potential energy and property surfaces in terms of cartesian normal modes.

Figure 5 compares different models to simulate IR, Raman, VCD and ROA spectra of (R)-4-F-2-azetidinone in the spectral range 300-1600 cm^{-1}, where both fundamental and non-fundamental transitions are present. It is clear that within the harmonic approximation, all bands are shifted and many transitions are missing with respect to fully anharmonic computations already for IR and Raman spectra, such deviations being further enhanced for VCD and ROA spectra. The situation is quite similar also once the anharmonic wavenumbers are combined with harmonic intensities since the positions of the fundamental transitions are significantly improved, but overtones and combination bands have still null

intensities and intensities of some fundamental bands are incorrect. As a result, in the present case fully harmonic and 'mixed' (anharmonic wavenumbers and harmonic intensities) simulations show quite similar band patterns for all spectroscopies. The situation is very different for the fully anharmonic spectra, which show several new transitions due to the overtones and combination bands together with significant intensity changes for some fundamental bands. In particular, all fully anharmonic spectra show a much richer structure within the 900-1200 cm^{-1} range with several non-fundamental bands (combinations involving $\gamma(R^{pucker})$, γ(N-H)+$\rho(CH_2)$, γ(C4)+β(C=O) and γ(C=O)+γ(NH)+$\rho(CH_2)$ vibrations124) of similar intensity to the fundamental transitions. Those effects might be less pronounced for low-resolution IR and Raman spectra, leading just to band broadening, but they modify also qualitatively the band shapes of VCD and ROA spectra due to positive and negative contributions of non-fundamental transitions. Moreover, for the ROA spectra the interaction between $\gamma(R^{pucker})$ (υ_{24}) and γ(N-H)+$\rho(CH_2)$(υ_{22}) leads to a non-negligible intensity of the corresponding combination band and further increases the intensity of the υ_{22} fundamental, resulting in two new distinct bands at 490 cm^{-1}(positive) and 399 cm^{-1} (negative), respectively.

These examples suggest that reliable comparative analysis of substituent or environmental effects on chiroptical spectra need to be performed at fully anharmonic level, and this will be analyzed in deeper detail in the next section for the series of (R)-4-X-2-azetidinone derivatives (X=F, Cl, Br).

4.3 Fully anharmonic IR, Raman, VCD and ROA spectra of (R)-4-X-2-azetidinones (X=F,Cl,Br)

Integrated studies combining several spectroscopic techniques allow to get a more complete and accurate picture of vibrational properties, along with their tuning by substituent and/or environmental effects. In fact, all vibrational spectroscopies share the same energy levels (hence the vibrational band positions), but the intensities of the different transitions change often strongly for IR, Raman, VCD, and ROA spectra. As a result, each of these different techniques shows different "fingerprint" regions and gives enhanced information for specific vibrational features. The consequent advantage of combining different spectroscopies is clearly demonstrated by comparison of IR, Raman, VCD and ROA spectra for the series of (R)-4-X-2-azetidinone derivatives (X-2az, X=F, Cl, Br), presented in Figure 6. The most intense IR features of all (R)-4-X-2-azetidinones are related to the C2=O6 stretching vibrations, at about 1838-1844 cm^{-1} and to the closely-lying non-fundamental transitions gaining intensity through anharmonic resonances. All IR spectra are very rich and show few distinct bands in the 300-1500 cm^{-1} and 2900-3500 cm^{-1} ranges. In the high-energy wing the position of the N1-H5 stretching vibration at 3426 cm^{-1} is not influenced by the halogen substituent, while the C4-H8 stretchings are shifted to higher energies and decrease in intensity with the increasing mass and electronegativity of the halogen. For Raman spectra, the most intense bands fall in the higher energy range, and are related to the N1-H5 and C-H stretchings, with the position and intensity of ν(C4-H8) showing a dependence on the halogen substituent analogous to that found in the IR spectrum. Moreover, the 300-600 cm^{-1} range, corresponding to the ring deformation vibrations involving halogen atoms present very different band patterns and the overall intensity increase from F to Cl and Br. The VCD

spectra show several intense features in the 300–1500 cm^{-1} range, with all other regions showing only very weak bands for all molecules. Moreover, F-2az shows many bands of similar intensity in the 300–1500 cm^{-1} range, while the VCD spectrum of Cl-2az shows two very strong transitions of opposite sign (negative at 608 cm^{-1} and positive at 979 cm^{-1}), with the latter band present also for Br-2az at 970 cm^{-1}. At variance with VCD, ROA spectra permit to analyze chiroptical properties also for the higher energy region, showing several very intense features in this spectral range. In particular, all spectra show a doublet of bands with opposite signs (positive+negative) at about 2900 cm^{-1} and single positive bands at about 3430 cm^{-1}. Interestingly, in this case the positive bands corresponding to the ν(C4-H8) stretching show essentially the same intensities for all halogens, whereas the negative $\nu(C3H_2)_{as}$ and positive ν(N1-H5) bands are influenced by the nature of the halogen atom, showing increasing intensities when going from F to Br. As a specific example, let us consider the close-lying bands of (R)-4-Br-2-azetidinone in the spectral range 470–540 cm^{-1}, marked by asterisks in Figure 7. In the IR spectrum, both β(C=O) (υ_{20}) at 477 cm^{-1} and γ(C=O)+γ(NH)(υ_{19}) at 537 cm^{-1} are rather weak, whereas their intensities increase in the Raman spectra, and thus can be more easily detected. These two vibrations show strong signals in both VCD and ROA spectra, which however differ by the sign, showing negative/positive and positive/negative patterns for VCD and ROA, respectively.

In our opinion, the comparative study sketched above demonstrates how several spectroscopic techniques can be analyzed within the same computational framework, also thanks to the integration of all tools in a virtual multifrequency spectrometer. In is noteworthy that spectral tuning by different halogens changes significantly for specific spectroscopic techniques, allowing a very detailed analysis of substituent effects by combining IR, Raman, VCD and ROA measurements with their theoretical fully anharmonic counterparts.

5 Conclusion

This paper reports the first full implementation of ROA spectra including both mechanical and electric/magnetic anharmonicities in the framework of generalized second-order vibrational perturbation theory taking full account of all first- and second-order resonances. Implementation of these new features in our virtual multifrequency spectrometer (VMS) allows comprehensive studies and vis-a-vis comparisons of simulated and experimental spectra for all the vibrational spectroscopies (IR, Raman, VCD, ROA). Although the present paper focuses on medium-size molecules in the gas phase, VMS can deal also with much larger systems thanks to the availability of reduced-dimensionality approaches and of effective continuum or discrete-continuum polarizable solvent models. After validation of the new tool for the well-studied methyloxirane benchmark, a comparative study of halogen-substituted azetidinones has been performed with the aim of revealing spectral tuning by closely related substituents with different mass, electronegativity, polarizability and/or steric hindrance. Our results point out the remarkable sensitivity to those parameters of all vibrational spectroscopies, and in particular of the chiral ones, thus paving the route to multi-spectroscopic characterization of subtle structural, stereo-electronic and, possibly, environmental effects. Although further developments are surely needed to extend such kind of studies from semirigid to flexible molecules, the results presented in this paper and in

parallel studies show, in our opinion, that we now possess of a robust tool for complementing experimental spectroscopic studies from both assignment and prediction points of view by means of direct vis-a-vis comparison between experimental spectra and those issuing from numerical simulations in which different effects can be selectively switched on and off.

Acknowledgement

The research leading to these results has received funding from the European Union's Seventh Framework Programme (FP7/2007-2013) under the grant agreement N° ERC-2012-AdG-320951-DREAMS. This work was supported by Italian MIUR (PRIN 2012 "STAR: Spectroscopic and computational Techniques for Astrophysical and atmospheric Research"). The high performance computer facilities of the DREAMS center (http://dreamshpc.sns.it) are acknowledged for providing computer resources. J.B. and M.B. also acknowledge the COST CMTS-Action CM1405 (MOLIM: MOLecules In Motion). The authors thank Professor Yunjie Xu and Professor Christian Merten for providing the experimental data of IR and VCD spectroscopic measurements of methyloxirane.

References

(1). Laane, J., editor. Frontiers of Molecular Spectroscopy. Elsevier; Amsterdam: 2009.

(2). Quack, M., Merkt, F., editors. Handbook of High-resolution Spectroscopy. John Wiley & Sons, Inc; 2011. p. 2182

(3). Siebert, F., Hildebrandt, P., editors. Vibrational Spectroscopy in Life Science. Wiley-VCH Verlag GmbH and Co. KGaA; Weinheim, Germany: 2008.

(4). Astrid, G.Rudolf, R., Jerker, W., editors. Single Molecule Spectroscopy in Chemistry, Physics and Biology: Nobel Symposium. Springer-Verlag; Berlin Heilderberg: 2010.

(5). Berova, N.Polavarapu, PL.Nakanishi, K., Woody, RW., editors. Comprehensive Chiroptical Spectroscopy: Instrumentation, Methodologies, and Theoretical Simulations. John Wiley & Sons, Inc.; Hoboken: New Jersey: 2012.

(6). Nafie, LA. Vibrational Optical Activity: Principles and Applications. John Wiley & Sons, Ltd; 2011.

(7). Magyarfalvi G, Tarczay G, Vass E. Vibrational Circular Dichroism. WIREs Comput Mol Sci. 2011; 1:403–425.

(8). Fausto, R., Khriachtchev, L., Hamm, P. Physics and Chemistry at Low Temperatures. Khriachtchev, L., editor. Pan Stanford Publishing Pte. Ltd; Singapore: 2011.

(9). Stephens, PJ., Devlin, FJ., Cheeseman, JR. VCD Spectroscopy for Organic Chemists. CRC Press, Taylor & Francis Group; Boca Raton, FL US: 2012.

(10). Nafie LA. Recent Advances in Linear and Nonlinear Raman Spectroscopy. Part VIII. J Raman Spectrosc. 2014; 45:1326–1346.

(11). Parchansky V, Kapitan J, Bouř P. Inspecting Chiral Molecules by Raman Optical Activity Spectroscopy. RSC Adv. 2014; 4:57125–57136.

(12). Alonso, JL., López, JC. Microwave Spectroscopy of Biomolecular Building Blocks. Topics in Current Chemistry. Springer; Berlin Heidelberg: 2015. p. 1-67.

(13). Rijs, AM., Oomens, J., editors. Topics in Current Chemistry. Vol. 364. Gas-Phase IR Spectroscopy and Structure of Biological Molecules. Springer International Publishing; 2015.

(14). Matysik, F-M., editor. Bioanalytical Reviews. Vol. 1. Advances in Chemical Bioanalysis. Springer Cham; Heidelberg New York Dordrecht London: 2014.

(15). Nicole L, Rozes L, Sanchez C. Integrative Approaches to Hybrid Multifunctional Materials: From Multidisciplinary Research to Applied Technologies. Adv Mater. 2010; 22:3208–3214. [PubMed: 20552603]

(16). Jensen, P., Bunker, PR. Computational Molecular Spectroscopy. John Wiley and Sons Ltd; Chichester, UK: 2000.

(17). Barone, V., editor. Computational Strategies for Spectroscopy, from Small Molecules to Nano Systems. John Wiley & Sons, Inc; Hoboken: New Jersey: 2011.

(18). Grunenberg, J., editor. Computational Spectroscopy. Wiley-VCH Verlag GmbH & Co. KGaA; Weinheim, Germany: 2010.

(19). Cappelli, C., Biczysko, M. Chapter Time-Independent Approach to Vibrational Spectroscopies. Computational Strategies for Spectroscopy, from Small Molecules to Nano Systems. Barone, V., editor. John Wiley & Sons, Inc; 2011. p. 309-360.

(20). Pedone A, Biczysko M, Barone V. Environmental Effects in Computational Spectroscopy: Accuracy and Interpretation. ChemPhysChem. 2010; 11:1812–1832. [PubMed: 20358575]

(21). Barron LD, Buckingham AD. Vibrational Optical Activity. Chem Phys Lett. 2010; 492:199–213.

(22). Puzzarini, C., Biczysko, M. Chapter Computational Spectroscopy Tools for Molecular Structure Analysis. Structure Elucidation in Organic Chemistry. Cid, MM., Bravo, J., editors. Wiley-VCH Verlag GmbH & Co. KGaA; 2015. p. 27-64.

(23). Barone V, Baiardi A, Biczysko M, Bloino J, Cappelli C, Lipparini F. Implementation and Validation of a Multi-purpose Virtual Spectrometer for Large Systems in Complex Environments. Phys Chem Chem Phys. 2012; 14:12404–12422. [PubMed: 22772710]

(24). Helgaker T, Coriani S, Jørgensen P, Kristensen K, Olsen J, Ruud K. Recent Advances in Wave Function-Based Methods of Molecular-Property Calculations. Chem Rev. 2012; 112:543–631. [PubMed: 22236047]

(25). Barone V, Biczysko M, Bloino J. Fully Anharmonic IR and Raman Spectra of Mediumsize Molecular Systems: Accuracy and Interpretation. Phys Chem Chem Phys. 2014; 16:1759–1787. [PubMed: 24346191]

(26). Pesonen, J., Halonen, L. Chapter Recent Advances in the Theory of Vibration-Rotation Hamiltonians. Adv Chem Phys. Vol. 125. John Wiley & Sons, Inc; 2003. p. 269-349.

(27). Császár AG, Fabri C, Szidarovszky T, Matyus E, Furtenbacher T, Czako G. The Fourth Age of Quantum Chemistry: Molecules in Motion. Phys Chem Chem Phys. 2012; 14:1085–1106. [PubMed: 21997300]

(28). Bowman JM. Beyond Platonic Molecules. Science. 2000; 290:724–725. [PubMed: 11184203]

(29). Carter S, Sharma AR, Bowman JM, Rosmus P, Tarroni R. Calculations of Rovibrational Energies and Dipole Transition Intensities for Polyatomic Molecules Using MULTIMODE. J Chem Phys. 2009; 131:224106. [PubMed: 20001023]

(30). Bowman JM, Carter S, Huang X. MULTIMODE: A Code to Calculate Rovibrational Energies of Polyatomic Molecules. Int Rev Phys Chem. 2003; 22:533–549.

(31). Carrington T, Wang X-G. Computing Ro-vibrational Spectra of Van Der Waals Molecules. WIREs Comput Mol Sci. 2011; 1:952–963.

(32). Rauhut G, Pulay P. Transferable Scaling Factors for Density Functional Derived Vibrational Force Fields. J Phys Chem. 1995; 99:3093–3100.

(33). Sinha P, Boesch SE, Gu C, Wheeler RA, Wilson AK. Harmonic Vibrational Frequencies: Scaling Factors for HF B3LYP, and MP2 Methods in Combination with Correlation Consistent Basis Sets. J Phys Chem A. 2004; 108:9213–9217.

(34). Andersson MP, Uvdal PE. New Scale Factors for Harmonic Vibrational Frequencies Using the B3LYP Density Functional Method with the Triple-ζ Basis Set 6-311+G(d,p). J Phys Chem A. 2005; 109:2937–2941. [PubMed: 16833612]

(35). Teixeira F, Melo A, Cordeiro MNDS. Calibration Sets and the Accuracy of Vibrational Scaling Factors: A Case Study with the X3LYP Hybrid Functional. J Chem Phys. 2010; 133:114109. [PubMed: 20866128]

(36). Alecu IM, Zheng J, Zhao Y, Truhlar DG. Computational Thermochemistry: Scale Factor Databases and Scale Factors for Vibrational Frequencies Obtained from Electronic Model Chemistries. J Chem Theory Comput. 2010; 6:2872–2887. [PubMed: 26616087]

(37). Katsyuba SA, Zvereva EE, Burganov TI. Is There a Simple Way to Reliable Simulations of Infrared Spectra of Organic Compounds? J Phys Chem A. 2013; 117:6664–6670. [PubMed: 23805975]

(38). Baker J, Jarzecki AA, Pulay P. Direct Scaling of Primitive Valence Force Constants:? An Alternative Approach to Scaled Quantum Mechanical Force Fields. J Phys Chem A. 1998; 102:1412–1424.

(39). Fabri C, Szidarovszky T, Magyarfalvi G, Tarczay G. Gas-Phase and Ar-Matrix SQM Scaling Factors for Various DFT Functionals with Basis Sets Including Polarization and Diffuse Functions. J Phys Chem A. 2011; 115:4640–4649. [PubMed: 21495661]

(40). Rauhut G, Hrenar T. A Combined Variational and Perturbational Study on the Vibrational Spectrum of P_2F_4. Chem Phys. 2008; 346:160–166.

(41). Heislbetz S, Rauhut G. Vibrational Multiconfiguration Self-consistent Field Theory: Implementation and Test Calculations. J Chem Phys. 2010; 132:124102. [PubMed: 20370109]

(42). Christiansen O. Selected New Developments in Vibrational Structure Theory: Potential Construction and Vibrational Wave Function Calculations. Phys Chem Chem Phys. 2012; 14:6672–6687. [PubMed: 22491444]

(43). Roy TK, Gerber RB. Vibrational Self-Consistent Field Calculations for Spectroscopy of Biological Molecules: New Algorithmic Developments and Applications. Phys Chem Chem Phys. 2013; 15:9468–9492. [PubMed: 23677257]

(44). Gaw, F., Willetts, A., Handy, N., Green, W. Advances in Molecular Vibrations and Collision Dynamics. Bowman, JM., editor. Vol. 1B. JAI Press; 1991. p. 169-185.

(45). Ruud K, Åstrand P-O, Taylor PR. An Efficient Approach for Calculating Vibrational Wave Functions and Zero-point Vibrational Corrections to Molecular Properties of Polyatomic Molecules. J Chem Phys. 2000; 112:2668–2683.

(46). Vázquez J, Stanton JF. Simple(r) Algebraic Equation for Transition Moments of Fundamental Transitions in Vibrational Second-order Perturbation Theory. Mol Phys. 2006; 104:377–388.

(47). Vázquez J, Stanton JF. Treatment of Fermi Resonance Effects on Transition Moments in Vibrational Perturbation Theory. Mol Phys. 2007; 105:101–109.

(48). Barone V. Anharmonic Vibrational Properties by a Fully Automated Second-order Perturbative Approach. J Chem Phys. 2005; 122 014108.

(49). Barone V. Vibrational Zero-point Energies and Thermodynamic Functions Beyond the Harmonic Approximation. J Chem Phys. 2004; 120:3059–3065. [PubMed: 15268458]

(50). Krasnoshchekov SV, Isayeva EV, Stepanov NF. Numerical-Analytic Implementation of the Higher-Order Canonical Van Vleck Perturbation Theory for the Interpretation of Medium-Sized Molecule Vibrational Spectra. J Phys Chem A. 2012; 116:3691–3709. [PubMed: 22369280]

(51). Hermes MR, Hirata S. Second-order Many-body Perturbation Expansions of Vibrational Dyson Self-energies. J Chem Phys. 2013; 139 034111.

(52). Rosnik AM, Polik WF. VPT2+K Spectroscopic Constants and Matrix Elements of the Transformed Vibrational Hamiltonian of a Polyatomic Molecule with Resonances using Van Vleck Perturbation Theory. Mol Phys. 2014; 112:261–300.

(53). Ringholm M, Jonsson D, Bast R, Gao B, Thorvaldsen AJ, Ekström U, Helgaker T, Ruud K. Analytic Cubic and Quartic Force Fields Using Density-Functional Theory. J Chem Phys. 2014; 140 034103.

(54). Bloino J. A VPT2 Route to Near-Infrared Spectroscopy: The Role of Mechanical and Electrical Anharmonicity. J Phys Chem A. 2015; 119:5269–5287. [PubMed: 25535769]

(55). Barone V, Biczysko M, Bloino J, Puzzarini C. Accurate Molecular Structures and Infrared Spectra of trans-2,3-dideuterooxirane, Methyloxirane, and trans-2,3-dimethyloxirane. J Chem Phys. 2014; 141 034107/1–17.

(56). Reva I, M Nunes C, Biczysko M, Fausto R. Conformational Switching in Pyruvic Acid Isolated in Ar and N2 Matrixes: Spectroscopic Analysis, Anharmonic Simulation, and Tunneling. J Phys Chem A. 2015; 119:2614–2627. [PubMed: 25332047]

(57). Barone V, Biczysko M, Bloino J, Cimino P, Penocchio E, Puzzarini C. CC/DFT Route toward Accurate Structures and Spectroscopic Features for Observed and Elusive Conformers of Flexible Molecules: Pyruvic Acid as a Case Study. J Chem Theory Comput. 2015; 11:4342–4363. [PubMed: 26575928]

(58). Cappelli C, Bloino J, Lipparini F, Barone V. Toward Ab Initio Anharmonic Vibrational Circular Dichroism Spectra in the Condensed Phase. J Phys Chem Lett. 2012; 3:1766–1773. [PubMed: 26291857]

(59). Barone V, Biczysko M, Bloino J, Puzzarini C. Glycine Conformers: a Never-ending Story? Phys Chem Chem Phys. 2013; 15:1358–1363. [PubMed: 23247893]

(60). Barone V, Biczysko M, Bloino J, Puzzarini C. The Performance of Composite Schemes and Hybrid CC/DFT Model in Predicting Structure, Thermodynamic and Spectroscopic Parameters: the Challenge of the Conformational Equilibrium in Glycine. Phys Chem Chem Phys. 2013; 15:10094–10111. [PubMed: 23599122]

(61). Barone V, Biczysko M, Bloino J, Puzzarini C. Characterization of the Elusive Conformers of Glycine from State-of-the-Art Structural, Thermodynamic, and Spectroscopic Computations: Theory Complements Experiment. J Chem Theory Comput. 2013; 9:1533–1547. [PubMed: 26587615]

(62). Barone V, Biczysko M, Puzzarini C. Quantum Chemistry Meets Spectroscopy for Astrochemistry: Increasing Complexity toward Prebiotic Molecules. Acc Chem Research. 2015; 48:1413–1422. [PubMed: 25894724]

(63). Egidi F, Bloino J, Cappelli C, Barone V. Development of a Virtual Spectrometer for Chiroptical Spectroscopies: The Case of Nicotine. Chirality. 2013; 25:701–708. [PubMed: 23857879]

(64). Barone V, Baiardi A, Bloino J. New Developments of a Multifrequency Virtual Spectrometer: Stereo-Electronic, Dynamical, and Environmental Effects on Chiroptical Spectra. Chirality. 2014; 26:588–600. [PubMed: 24839096]

(65). Bloino J, Biczysko M, Barone V. General Perturbative Approach for Spectroscopy, Thermodynamics, and Kinetics: Methodological Background and Benchmark Studies. J Chem Theory Comput. 2012; 8:1015–1036. [PubMed: 26593363]

(66). Bloino J, Barone V. A Second-order Perturbation Theory Route to Vibrational Averages and Transition Properties of Molecules: General Formulation and Application to Infrared and Vibrational Circular Dichroism Spectroscopies. J Chem Phys. 2012; 136:124108. [PubMed: 22462836]

(67). Piccardo M, Bloino J, Barone V. Generalized Vibrational Perturbation Theory for Rotovibrational Energies of Linear, Symmetric and Asymmetric Tops: Theory, Approximations and Automated Approaches to Deal with Medium-to-Large Molecular Systems. Int J Quantum Chem. 2015; 115:948–982. [PubMed: 26345131]

(68). Barone V, Bloino J, Biczysko M, Santoro F. Fully Integrated Approach to Compute Vibrationally Resolved Optical Spectra: From Small Molecules to Macrosystems. J Chem Theory Comput. 2009; 5:540–554. [PubMed: 26610221]

(69). Bloino J, Biczysko M, Santoro F, Barone V. General Approach to Compute Vibrationally Resolved One-Photon Electronic Spectra. J Chem Theory Comput. 2010; 6:1256–1274.

(70). Baiardi A, Bloino J, Barone V. General Time Dependent Approach to Vibronic Spectroscopy Including Franck–Condon, Herzberg–Teller, and Duschinsky Effects. J Chem Theory Comput. 2013; 9:4097–4115. [PubMed: 26592403]

(71). Baiardi A, Bloino J, Barone V. A General Time-dependent Route to Resonance-Raman Spectroscopy Including Franck-Condon, Herzberg-Teller and Duschinsky Effects. J Chem Phys. 2014; 141:114108. [PubMed: 25240346]

(72). Carnimeo I, Puzzarini C, Tasinato N, Stoppa P, Charmet AP, Biczysko M, Cappelli C, Barone V. Anharmonic Theoretical Simulations of Infrared Spectra of Halogenated Organic Compounds. J Chem Phys. 2013; 139:074310. [PubMed: 23968095]

(73). Latouche C, Palazzetti F, Skouteris D, Barone V. High-Accuracy Vibrational Computations for Transition-Metal Complexes Including Anharmonic Corrections: Ferrocene, Ruthenocene, and Osmocene as Test Cases. J Chem Theory Comput. 2014; 10:4565–4573. [PubMed: 26588150]

(74). Carnimeo I, Biczysko M, Bloino J, Barone V. Reliable Structural, Thermodynamic, and Spectroscopic Properties of Organic Molecules Adsorbed on Silicon Surfaces from Computational Modeling: the Case of Glycine@Si(100). Phys Chem Chem Phys. 2011; 13:16713–16727. [PubMed: 21858336]

(75). Fornaro T, Carnimeo I, Biczysko M. Towards Feasible and Comprehensive Computational Protocol for Simulation of the Spectroscopic Properties of Large Molecular Systems: The Anharmonic Infrared Spectrum of Uracil in the Solid State by Reduced Dimensionality/Hybrid VPT2 Approach. J Phys Chem A. 2015; 119:5313–5326. [PubMed: 25474755]

(76). Merten C, Bloino J, Barone V, Xu Y. Anharmonicity Effects in the Vibrational CD Spectra of Propylene Oxide. J Phys Chem Lett. 2013; 4:3424–3428.

(77). Cappelli C, Monti S, Scalmani G, Barone V. On the Calculation of Vibrational Frequencies for Molecules in Solution Beyond the Harmonic Approximation. J Chem Theory Comput. 2010; 6:1660–1669. [PubMed: 26615698]

(78). Sunahori FX, Su Z, Kang C, Xu Y. Infrared Diode Laser Spectroscopic Investigation of Four C-H Stretching Vibrational Modes of Propylene Oxide. Chem Phys Lett. 2010; 494:14–20.

(79). Sebestik J, Bouř P. Raman Optical Activity of Methyloxirane Gas and Liquid. J Phys Chem Lett. 2011; 2:498–502.

(80). Polavarapu PL, Hess BA, Schaad LJ. Vibrational Spectra of Epoxypropane. J Chem Phys. 1985; 82:1705–1710.

(81). Crawford T. Ab Initio Calculation of Molecular Chiroptical Properties. Theor Chem Acc. 2006; 115:227–245.

(82). Coriani S, Thorvaldsen AJ, Kristensen K, Jørgensen P. Variational Response-Function Formulation of Vibrational Circular Dichroism. Phys Chem Chem Phys. 2011; 13:4224–4229. [PubMed: 21283895]

(83). Mehta PD, Sengar N, Pathak A. 2-Azetidinone: A New Profile of Various Pharmacological Activities. Eur J Med Chem. 2010; 45:5541–5560. [PubMed: 20970895]

(84). Rode JE, Dobrowolski JC. Density Functional IR, Raman, and VCD Spectra of Halogen Substituted β-lactams. J Molec Structure. 2003:651–653. 705–717.

(85). Vidal LN, Egidi F, Barone V, Cappelli C. Origin Invariance in Vibrational Resonance Raman Optical Activity. J Chem Phys. 2015; 142:174101. [PubMed: 25956084]

(86). Nafie LA. Theory of Resonance Raman Optical Activity: the Single Electronic State Limit. Chem Phys. 1996; 205:309–322.

(87). Barron LD, Buckingham AD. Rayleigh and Raman Scattering From Optically Active Molecules. Mol Phys. 1971; 20:1111–1119.

(88). Barron LD, Buckingham AD. Rayleigh and Raman Optical Activity. Annu Rev Phys Chem. 1975; 26:381–396.

(89). Nafie LA. Infrared and Raman Vibrational Optical Activity: Theoretical and Experimental Aspects. Annu Rev Phys Chem. 1997; 48:357–386. [PubMed: 9348659]

(90). Barron LD, Hecht L, McColl IH, Blanch EW. Raman Optical Activity Comes of Age. Mol Phys. 2004; 102:731–744.

(91). Barron, LD. Molecular Light Scattering and Optical Activity. 2nd ed. Cambridge University Press; 2004.

(92). Ruud K, Thorvaldsen AJ. Theoretical Approaches to the Calculation of Raman Optical Activity Spectra. Chirality. 2009; 21:E54–E67. [PubMed: 19750498]

(93). Hecht L, Nafie LA. Theory of Natural Raman Optical Activity. Mol Phys. 1991; 72:441–469.

(94). Cheeseman JR, Frisch MJ, Devlin FJ, Stephens PJ. Ab Initio Calculation of Atomic Axial Tensors and Vibrational Rotational Strengths Using Density Functional Theory. Chem Phys Lett. 1996; 252:211–220.

(95). Martin JML, Lee TJ, Taylor PM, François J-P. The Anharmonic Force Field of Ethylene, C_2H_4, by Means of Accurate ab initio Calculations. J Chem Phys. 1995; 103:2589–2602.

(96). Matthews DA, Stanton JF. Quantitative Analysis of Fermi Resonances by Harmonic Derivatives of Perturbation Theory Corrections. Mol Phys. 2009; 107:213–222.

(97). Darling BT, Dennison DM. The Water Vapor Molecule. Phy Rev. 1940; 57:128–139.

(98). Lehmann KK. Beyond the x-K Relations. Mol Phys. 1989; 66:1129–1137.

(99). Martin JML, Taylor PM. Accurate Ab Initio Quartic Force Field for trans-HNNH and Treatment of Resonance Polyads. Spectrochim Acta A. 1997; 53:1039–1050.

(100). Hänninen V, Halonen L. Calculation of Spectroscopic Parameters and Vibrational Overtones of Methanol. Mol Phys. 2003; 101:2907–2916.

(101). Matthews DA, Vázquez J, Stanton JF. Calculated Stretching Overtone Levels and Darling-Dennison Resonances in Water: a Triumph of Simple Theoretical Approaches. Mol Phys. 2007; 105:2659–2666.

(102). Krasnoshchekov SV, Vogt N, Stepanov NF. Ab Initio Anharmonic Analysis of Vibrational Spectra of Uracil Using the Numerical-Analytic Implementation of Operator Van Vleck Perturbation Theory. J Phys Chem A. 2015; 119:6723–6737. [PubMed: 26020099]

(103). Krasnoshchekov SV, Isayeva EV, Stepanov NF. Criteria for First- and Second-order Vibrational Resonances and Correct Evaluation of the Darling-Dennison Resonance Coefficients Using the Canonical Van Vleck Perturbation Theory. J Chem Phys. 2014; 141:234114. [PubMed: 25527926]

(104). Piccardo M, Penocchio E, Puzzarini C, Biczysko M, Barone V. Semi-Experimental Equilibrium Structure Determinations by Employing B3LYP/SNSD Anharmonic Force Fields: Validation and Application to Semirigid Organic Molecules. J Phys Chem A. 2015; 119:2058–2082. [PubMed: 25648634]

(105). Biczysko M, Bloino J, Brancato G, Cacelli I, Cappelli C, Ferretti A, Lami A, Monti S, Pedone A, Prampolini G, et al. Integrated Computational Approaches for Spectroscopic Studies of Molecular Systems in the Gas Phase and in Solution: Pyrimidine as a Test Case. Theor Chem Acc. 2012; 131 1201/1–19.

(106). Puzzarini C, Biczysko M, Barone V. Accurate Harmonic/Anharmonic Vibrational Frequencies for Open-Shell Systems: Performances of the B3LYP/N07D Model for Semirigid Free Radicals Benchmarked by CCSD(T) Computations. J Chem Theory Comput. 2010; 6:828–838. [PubMed: 26613310]

(107). Puzzarini C, Biczysko M, Barone V. Accurate Anharmonic Vibrational Frequencies for Uracil: The Performance of Composite Schemes and Hybrid CC/DFT Model. J Chem Theory Comput. 2011; 7:3702–3710. [PubMed: 26598265]

(108). Becke AD. Density-functional Thermochemistry. III. The Role of Exact Exchange. J Chem Phys. 1993; 98:5648–5652.

(109). Double and triple-ζ basis sets of SNS family. are available in the Download section. http://dreams.sns.it, (last visited: November 16, 2015)

(110). Bergner A, Dolg M, Kuchle W, Stoll H, Preuss H. Ab-initio Energy-Adjusted Pseudopotentials for Elements of Groups 13-17. Mol Phys. 1993; 80:1431.

(111). Igelmann G, Stoll, Preuss H. Pseudopotentials for Main Group Elements (IIIA Through VIIA). Mol Phys. 1988; 65:1321.

(112). Dunning TH. Gaussian Basis Sets for Use in Correlated Molecular Calculations. I. The Atoms Boron through Neon and Hydrogen. J Chem Phys. 1989; 90:1007.

(113). Begue D, Carbonniere P, Barone V, Pouchan C. Performance of ab initio and DFT/PCM Methods in Calculating Vibrational Spectra in Solution: Formaldehyde in Acetonitrile as a Test Case. Chem Phys Lett. 2005; 416:206–211.

(114). Begue D, Carbonniere P, Pouchan C. Calculations of Vibrational Energy Levels by Using a Hybrid ab Initio and DFT Quartic Force Field: Application to Acetonitrile. J Phys Chem A. 2005; 109:4611–4616. [PubMed: 16833799]

(115). Raghavachari K, Trucks GW, Pople JA, Head-Gordon M. A Fifth-order Perturbation Comparison of Electron Correlation Theories. Chem Phys Lett. 1989; 157:479–483.

(116). Kendall A, Dunning TH Jr, Harrison RJ. Electron Affinities of the First-row Atoms Revisited. Systematic Basis Sets and Wave Functions. J Chem Phys. 1992; 96:6796–6806.

(117). Woon DE, Dunning TH Jr. Gaussian Basis Sets for Use in Correlated Molecular Calculations. V. Core-valence Basis Sets for Boron through Neon. J Chem Phys. 1995; 103:4572–4585.

(118). Frisch, MJ., Trucks, GW., Schlegel, HB., Scuseria, GE., Robb, MA., Cheeseman, JR., Scalmani, G., Barone, V., Mennucci, B., Petersson, GA., et al. Gaussian Development Version, Revision I. 03. Gaussian, Inc; Wallingford CT: 2015.

Europe PMC Funders Author Manuscripts

(119). Licari D, Baiardi A, Biczysko M, Egidi F, Latouche C, Barone V. Implementation of a Graphical User Interface for the Virtual Multifrequency Spectrometer: The VMS-Draw Tool. J Comput Chem. 2015; 36:321–334. [PubMed: 25408126]

(120). Crawford TD, Ruud K. Coupled-Cluster Calculations of Vibrational Raman Optical Activity Spectra. ChemPhysChem. 2011; 12:3442–3448. [PubMed: 21919183]

(121). Cheeseman JR, Frisch MJ. Basis Set Dependence of Vibrational Raman and Raman Optical Activity Intensities. J Chem Theory Comput. 2011; 7:3323–3334. [PubMed: 26598166]

(122). Halls MD, Schlegel HB. Comparison Study of the Prediction of Raman Intensities Using Electronic Structure Methods. J Chem Phys. 1999; 111:8819–8824.

(123). Neugebauer J, Reiher M, Hess BA. Coupled-Cluster Raman Intensities: Assessment and Comparison with Multiconfiguration and Density Functional Methods. J Chem Phys. 2002; 117:8623–8633.

(124). Approximate description: ν-stretching, δ-scissoring, β-bending, ρ-rocking, τ-twisting, ω-wagging, γ-out of plane, s-symmetric, as-asymmetric, R-ring, R^{breath}-ring-breathing, R^{pucker}-ring-puckering. Notation and assignment adopted from Ref..84

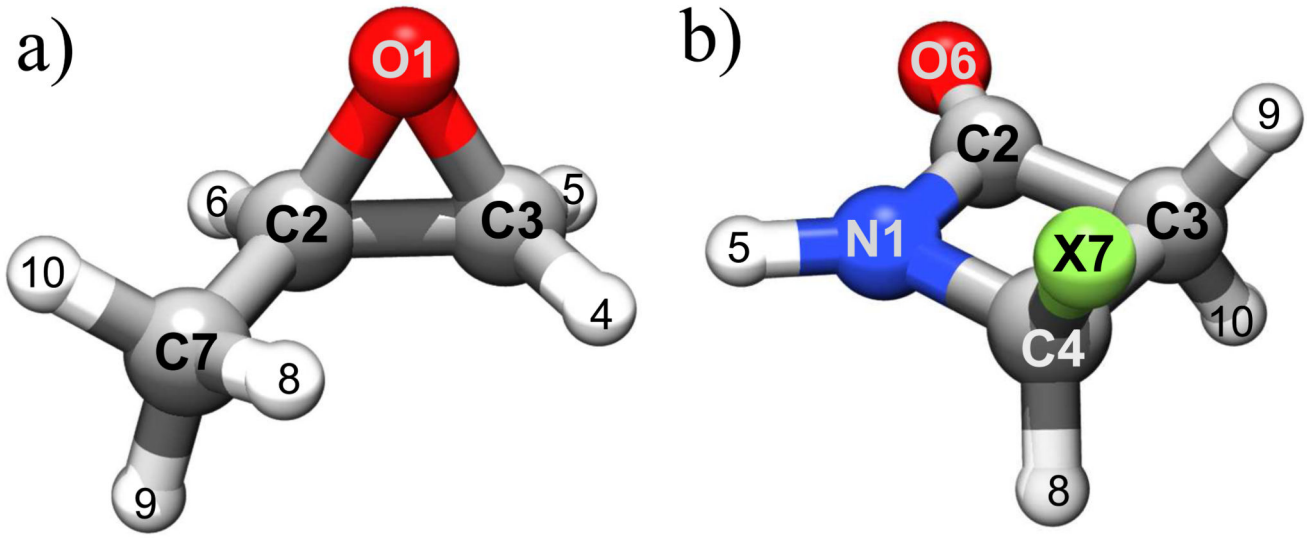

Figure 1.
Molecular structures of methyloxirane (a) and 4-X-2-azetidinones (X=F, Cl, Br) (b) along with the atom labelling in line with references55 and, 84 respectively.

Europe PMC Funders Author Manuscripts

Europe PMC Funders Author Manuscripts

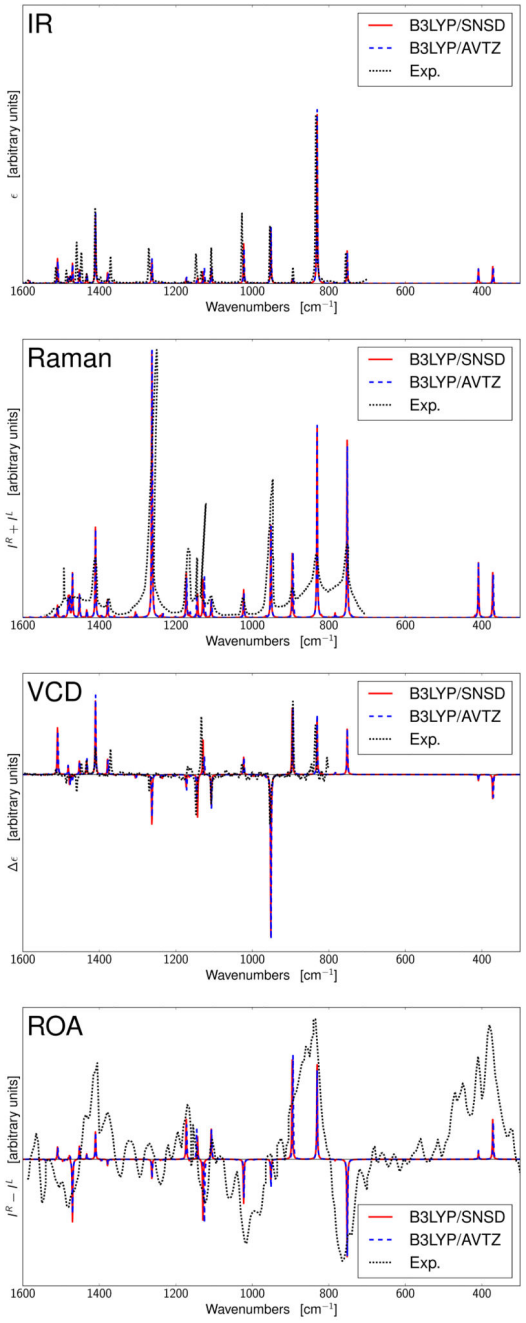

Figure 2.

Fully anharmonic IR, Raman, VCD and ROA spectra of (R)-methyloxirane compared to their experimental counterparts measured in low-temperature Ar Matrix (IR, VCD76) or gas phase (Raman, ROA79). Vibrational wavenumbers have been computed at the “cheapCC”/B3LYP level55 in conjunction with B3LYP intensities. B3LYP computations have been performed with the SNSD and aug-cc-pVTZ (AVTZ) basis sets. All spectra have been convoluted by means of Lorentzian distribution functions with FWHM of 2 cm^{-1}. 36

Europe PMC Funders Author Manuscripts

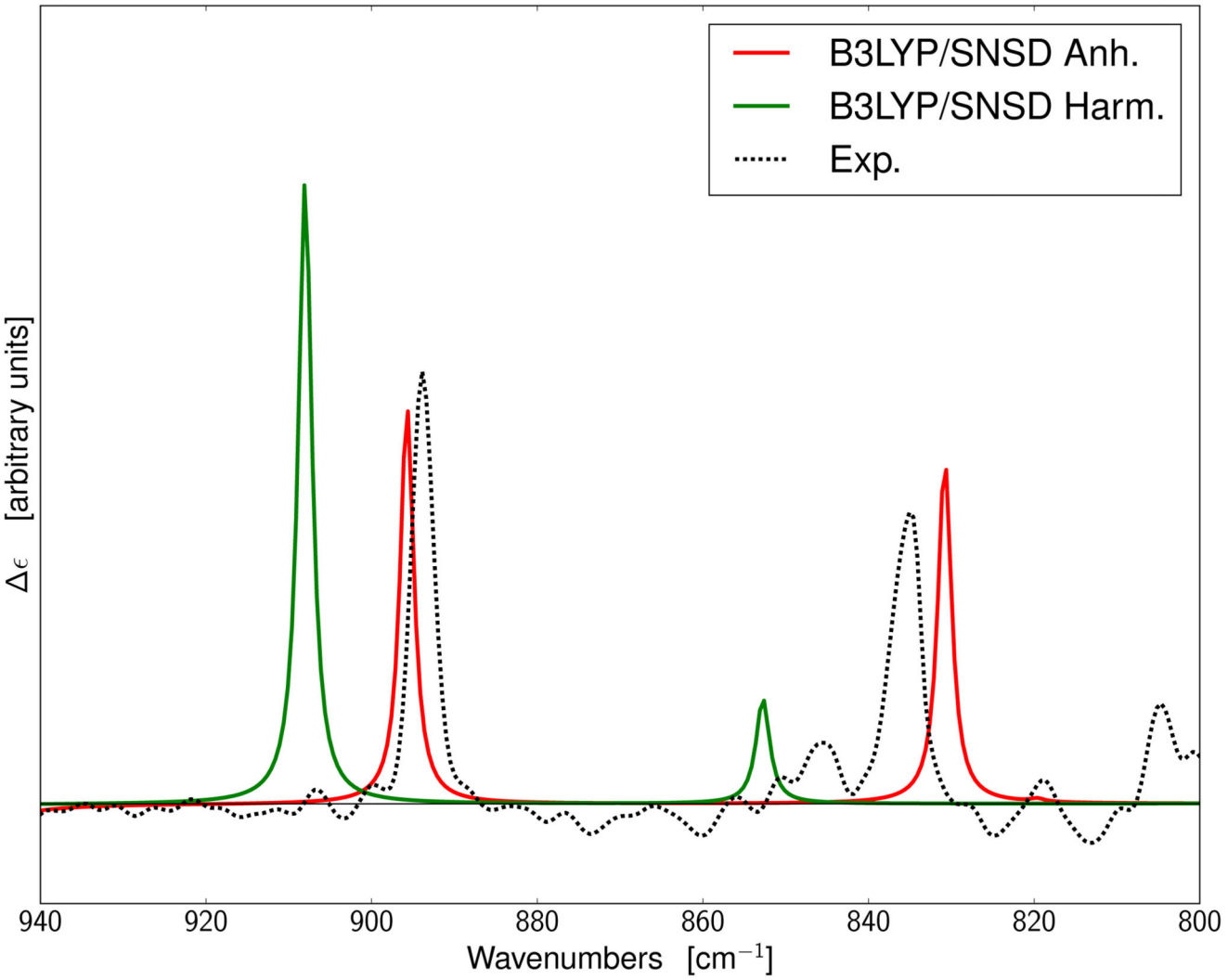

Figure 3.

Harmonic and fully anharmonic VCD spectra of (R)-methyloxirane in the 800–940 cm^{-1} range compared to experiment.76 Harmonic wavenumbers have been computed at the "cheapCC" level55 and combined with anharmonic corrections at the B3LYP/SNSD level. VCD harmonic and anharmonic intensities are computed at B3LYP/SNSD level. All spectra have been convoluted by means of Lorentzian distribution functions with FWHM of 2 cm^{-1}.

Europe PMC Funders Author Manuscripts

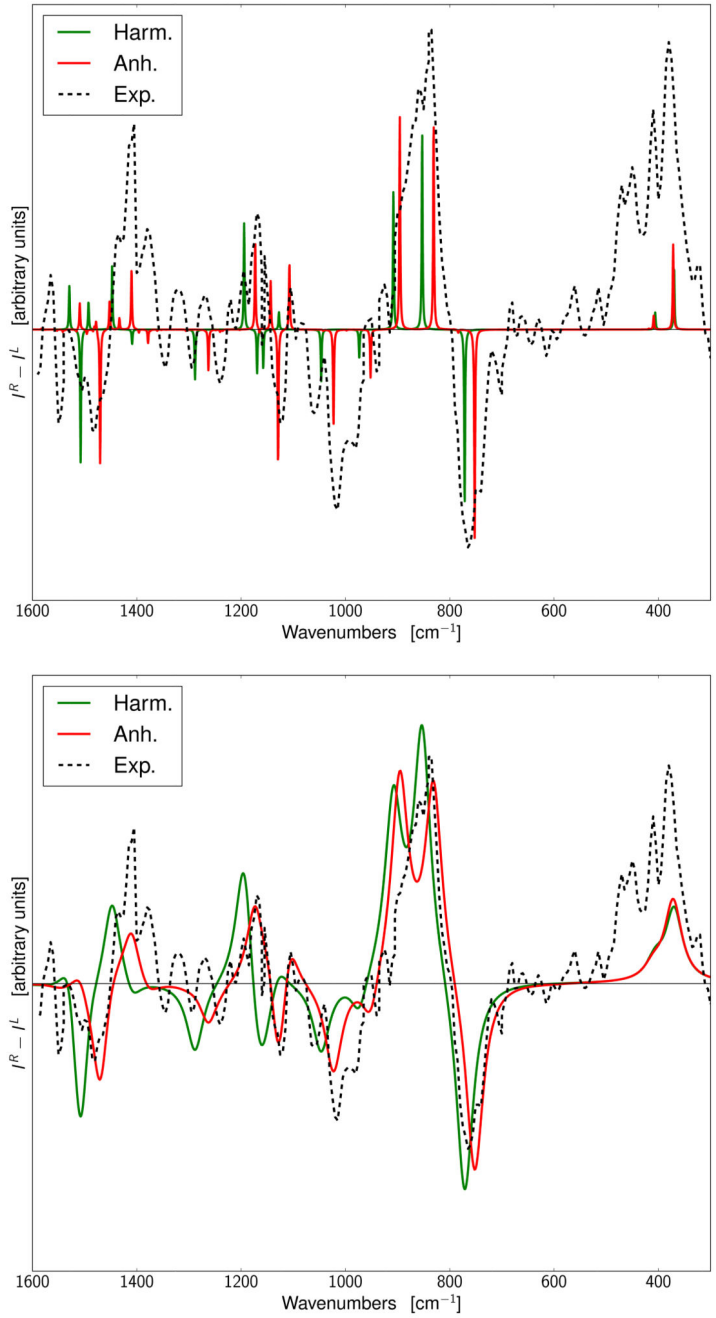

Figure 4.

Harmonic and fully anharmonic ROA spectra of (R)-methyloxirane compared to its experimental counterpart (in the gas phase79). Harmonic wavenumbers have been computed at the “cheapCC” level55 and combined with anharmonic corrections at the B3LYP/SNSD level. ROA harmonic and anharmonic intensities are computed at B3LYP/SNSD level. Theoretical spectra have been convoluted by means of Lorentzian distribution functions with FWHM of 2 cm^{-1} (upper panel) and of 40 cm^{-1} (lower panel).

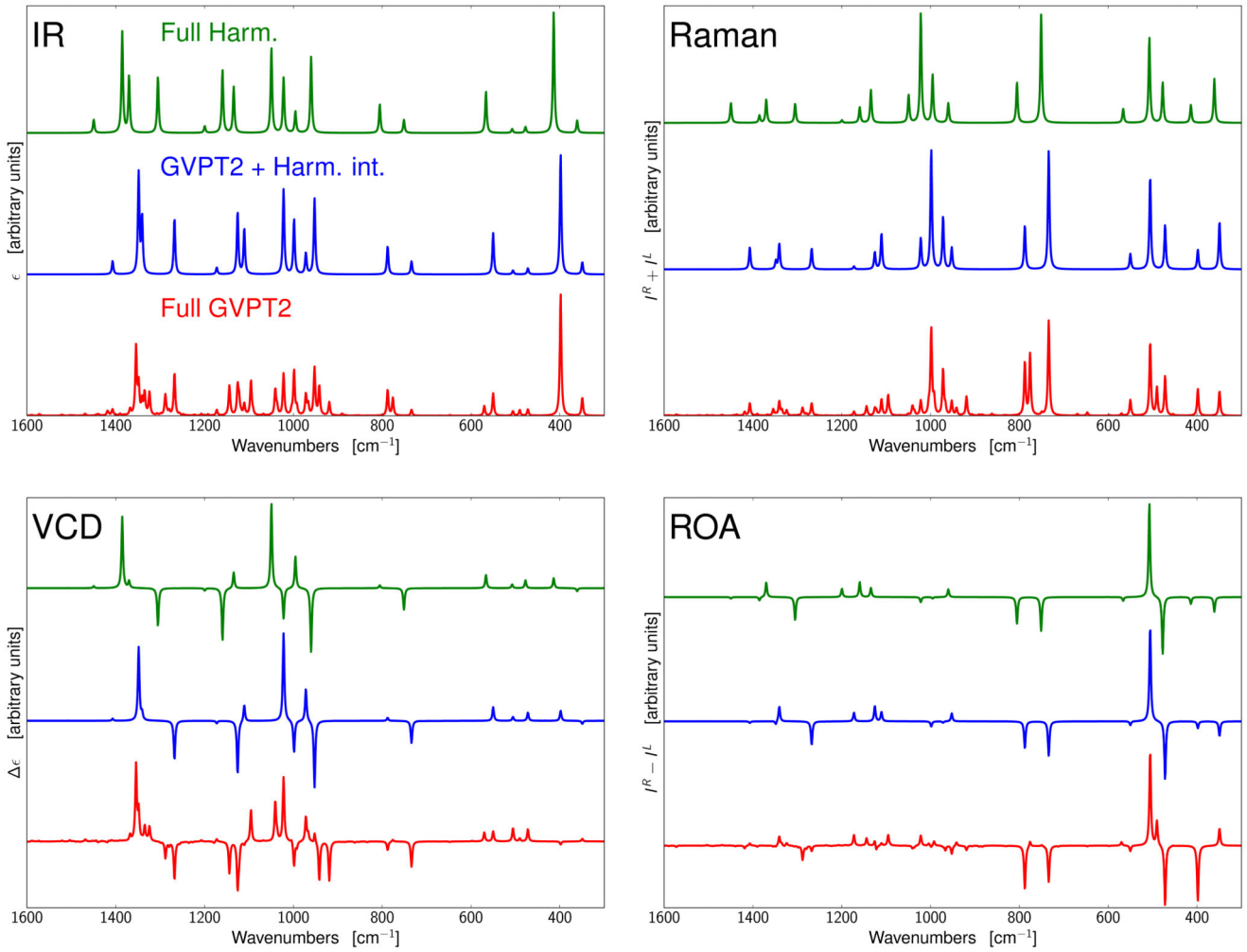

Figure 5.

Theoretical IR, VCD, Raman and ROA spectra of (R)-4-fluoro-2-azetidinone in the 300–1600 cm^{-1} range. Fully harmonic (harmonic energies and intensities) spectra (red, upper traces), spectra obtained by combining anharmonic wavenumbers with harmonic intensities (blue, middle traces) and fully anharmonic (anharmonic energies and intensities) spectra (green, lower traces). All computations have been performed at the B3LYP/SNSD level, and the computed lines have been convoluted by means of Lorentzian distribution functions with FWHM of 4 cm^{-1}.

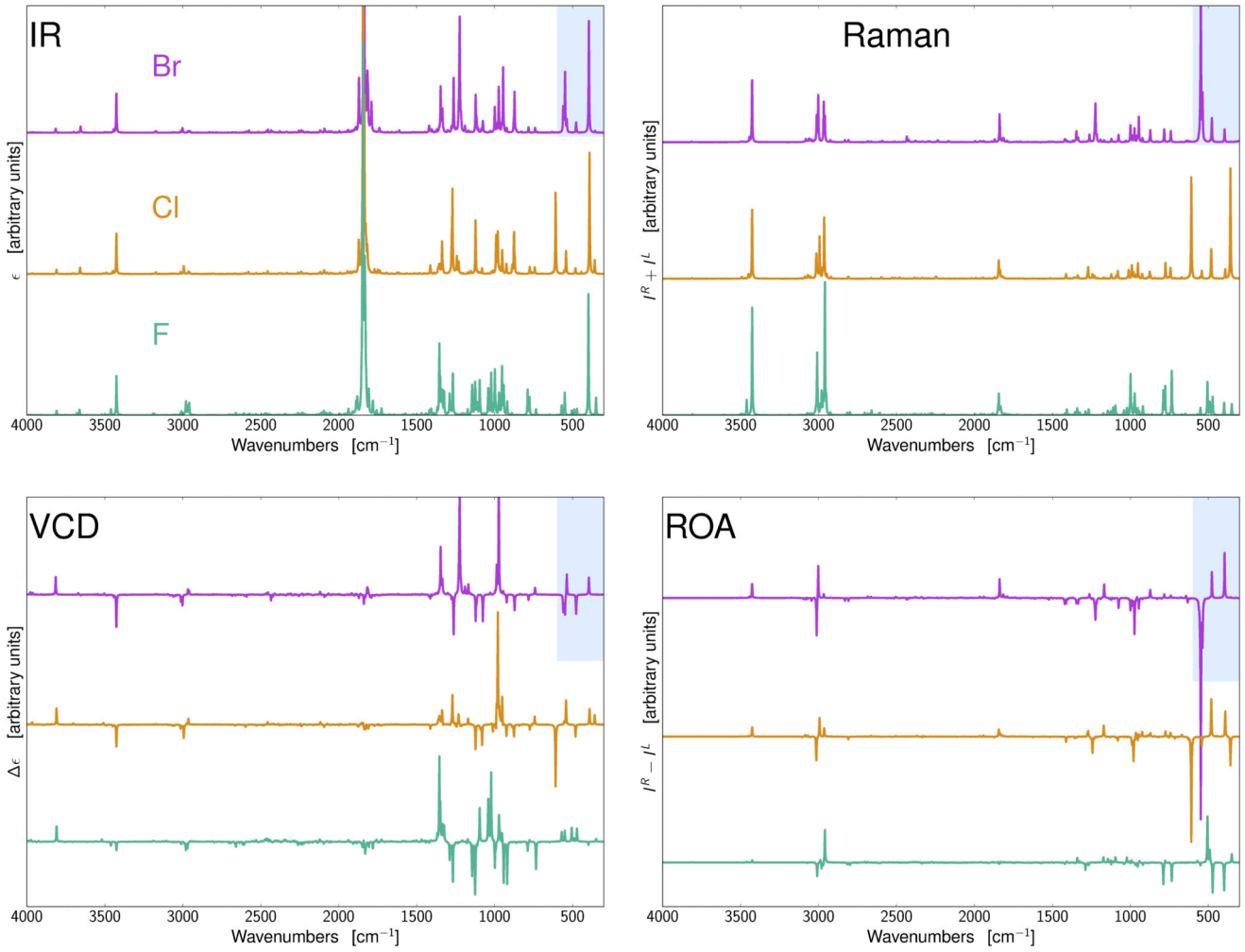

Figure 6.

Fully anharmonic IR, VCD, Raman and ROA spectra of (R)-4-X-2-azetidinones (X=F, Cl, Br) in the 300–4000 cm^{-1} range. All computations have been performed at the B3LYP/SNSD level, and the computed lines have been convoluted by means of Lorentzian distribution functions with FWHM of 4 cm^{-1}.

Europe PMC Funders Author Manuscripts

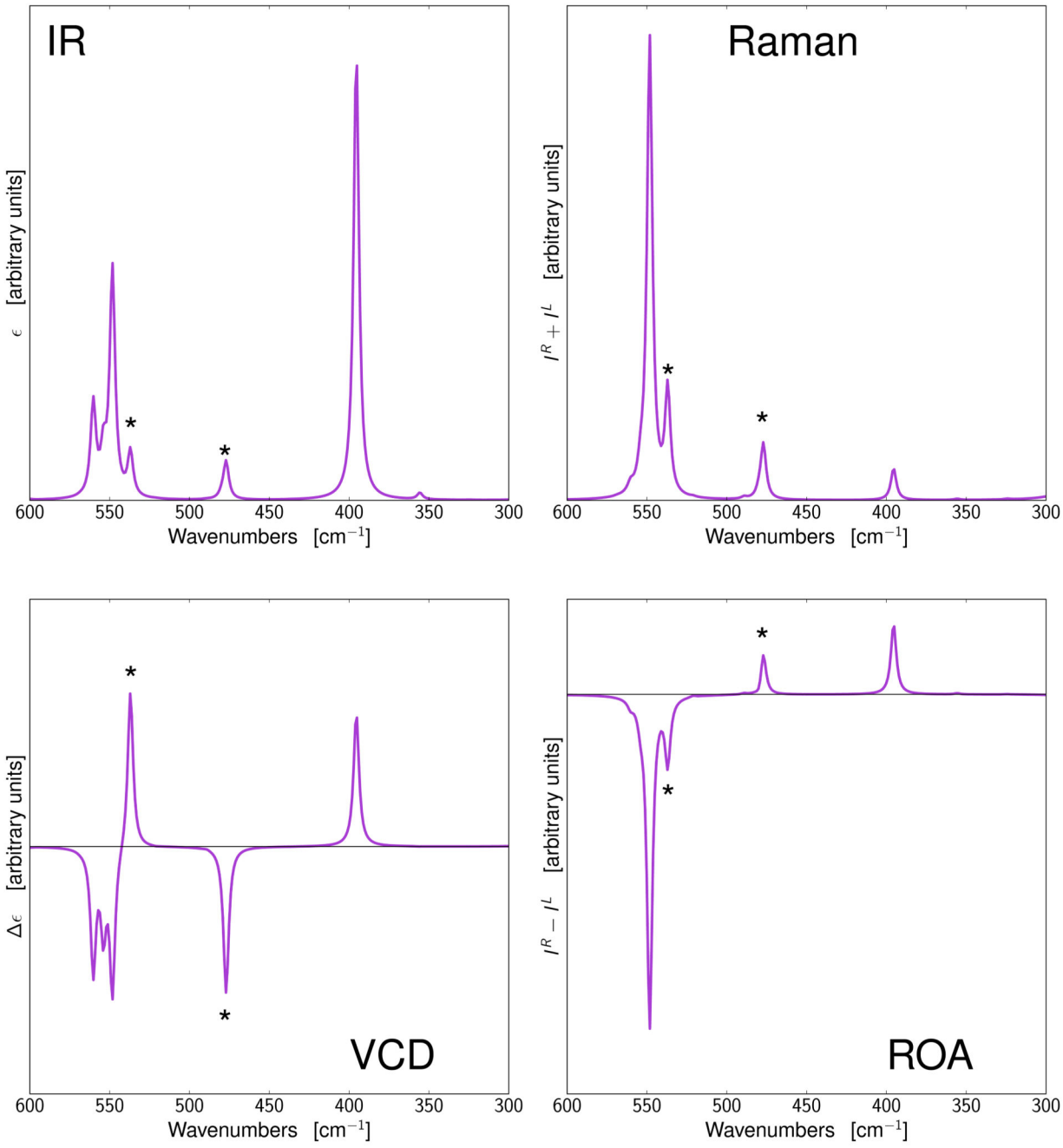

Figure 7.

Fully anharmonic IR, VCD, Raman and ROA spectra of (R)-4-Br-azetidinone in the 300–600 cm^{-1} range, highlighted in light blue in Figure 6. υ_{19} and υ_{20} vibrations are marked by asterisks. All computations have been performed at the B3LYP/SNSD level, and the computed lines have been convoluted by means of Lorentzian distribution functions with FWHM of 4 cm^{-1}.

Europe PMC Funders Author Manuscripts

Table 1

Description of the most common type of scattering geometries and polarizations.

Symbol	Description
$\Delta(0°)$	forward scattering
$\Delta(180°)$	backward scattering
$\Delta^z(90°)$	depolarized right-angle scattering, where the scattering direction is at right angle with respect to the incident beam and the transmission axis of the linear polarization analyzer, placed on the path of the scattered beam (for ICP) or the incident beam (for SCP), is parallel to the scattering plane (*yz*)
$\Delta^x(90°)$	polarized right-angle scattering, same as $\Delta^z(90°)$ but the transmission axis of the linear polarization analyzer is perpendicular to the scattering plane
$\Delta^*(90°)$	magic-angle right-angle scattering, same as $\Delta^z(90°)$ but the transmission axis of the linear polarization analyzer is set at the "magic angle" of $\pm \sin^{-1}(2/3)^1/2 \approx \pm 54.74°$ to the scattering plane to remove the contribution from the electric dipole-electric quadrupole (*magic angle* CID)

Europe PMC Funders Author Manuscripts

Table 2

Equations for the most common types of scattering in ROA.

K is a term related to the experimental setup, proportional to the fourth power of the scattered energy, c is the speed of light.

Scattering	$I^R - I^L$	$I^R + I^L$
$\Delta_{SCP}(0°)$	$\frac{8K}{c}[90\alpha G' + 2\beta(G')^2 - 2\beta(A)^2]$	$4K[45\alpha^2 + 7\beta(\alpha)^2]$
$\Delta^x_{SCP}(90°)$	$\frac{4K}{c}[45\alpha G' + 7\beta(G')^2 + \beta(A)^2]$	$2K[45\alpha^2 + 7\beta(\alpha)^2]$
$\Delta^*_{SCP}(90°)$	$\frac{40K}{3c}[9\alpha G' + 2\beta(G')^2]$	$\frac{20K}{3}[9\alpha^2 + 2\beta(\alpha)^2]$
$\Delta^z_{SCP}(90°)$	$\frac{8K}{c}[3\beta(G')^2 - \beta(A)^2]$	$4K[3\beta(\alpha)^2]$
$\Delta_{SCP}(180°)$	$\frac{8K}{c}[12\beta(G')^2 + 4\beta(A)^2]$	$4K[45\alpha^2 + 7\beta(\alpha)^2]$
$\Delta_{DCP_I}(180°)$	$\frac{16K}{c}[6\beta(G')^2 + 2\beta(A)^2]$	$24K\beta(\alpha)^2$

Europe PMC Funders Author Manuscripts

Table 3

Equivalence relations between the model property $\boldsymbol{P}$ and actual properties $\boldsymbol{\alpha}$, $\boldsymbol{G'}$ and $\boldsymbol{A}$. The electric ($\boldsymbol{\mu}$) and magnetic ($\boldsymbol{m}$) dipoles, used in IR and VCD intensities, are also reported. $\boldsymbol{M}$ is the atomic axial tensor (AAT).94

P	P_0	P_i	P_{ji}	P_{jki}	s_0	s_1	s_2	S
$\boldsymbol{\mu}$	$\boldsymbol{\mu}^{\mathrm{eq}}$	$\frac{\partial \boldsymbol{\mu}}{\partial q_i}$	$\frac{\partial^2 \boldsymbol{\mu}}{\partial q_i q_j}$	$\frac{\partial^3 \boldsymbol{\mu}}{\partial q_i q_j q_k}$	$\frac{1}{\sqrt{2}}$	$\frac{1}{2\sqrt{2}}$	$\frac{1}{6\sqrt{2}}$	+1
$\boldsymbol{m}$	$\boldsymbol{0}$	$\boldsymbol{M}_i$	$\frac{\partial \boldsymbol{M}_i}{\partial q_j}$	$\frac{\partial^2 \boldsymbol{M}_i}{\partial q_j q_k}$	$\frac{\imath\hbar}{\sqrt{2}}$	$\frac{\imath\hbar}{\sqrt{2}}$	$\frac{\imath\hbar}{\sqrt{2}}$	−1
$\boldsymbol{\alpha}$	$\boldsymbol{\alpha}^{\mathrm{eq}}$	$\frac{\partial \boldsymbol{\alpha}}{\partial q_i}$	$\frac{\partial^2 \boldsymbol{\alpha}}{\partial q_i q_j}$	$\frac{\partial^3 \boldsymbol{\alpha}}{\partial q_i q_j q_k}$	$\frac{1}{\sqrt{2}}$	$\frac{1}{2\sqrt{2}}$	$\frac{1}{6\sqrt{2}}$	+1
$\boldsymbol{G'}$	$\boldsymbol{G'}^{\mathrm{eq}}$	$\frac{\partial \boldsymbol{G'}}{\partial q_i}$	$\frac{\partial^2 \boldsymbol{G'}}{\partial q_i q_j}$	$\frac{\partial^3 \boldsymbol{G'}}{\partial q_i q_j q_k}$	$\frac{1}{\sqrt{2}}$	$\frac{1}{2\sqrt{2}}$	$\frac{1}{6\sqrt{2}}$	+1
$\boldsymbol{A}$	$\boldsymbol{A}^{\mathrm{eq}}$	$\frac{\partial \boldsymbol{A}}{\partial q_i}$	$\frac{\partial^2 \boldsymbol{A}}{\partial q_i q_j}$	$\frac{\partial^3 \boldsymbol{A}}{\partial q_i q_j q_k}$	$\frac{1}{\sqrt{2}}$	$\frac{1}{2\sqrt{2}}$	$\frac{1}{6\sqrt{2}}$	+1